




Article

Single Fiber Reflectance Spectroscopy for the Monitoring of Cement Paste

Pedro M. da Silva ¹, Luís C. C. Coelho ^{1,2,*} and José M. M. M. de Almeida ^{1,3}

- ¹ INESC TEC-Institute for Systems and Computer Engineering, Technology and Science and Faculty of Sciences, University of Porto, Rua do Campo Alegre, 4169-007 Porto, Portugal; pedro.m.madeira@inesctec.pt (P.M.d.S.); jmma@utad.pt (J.M.M.M.d.A.)
- ² Department of Physics and Astronomy, Faculty of Sciences, University of Porto, Rua do Campo Alegre, 4169-007 Porto, Portugal
- ³ Department of Physics, School of Sciences and Technology, University of Trás-os-Montes e Alto Douro, 5001-801 Vila Real, Portugal
- * Correspondence: lcoelho@inesctec.pt

Abstract: Reinforced concrete structures are an essential part of our modern society, and monitoring their structural health is of paramount importance. Early detection of decay allows for the reduction of repair costs and, more importantly, the prevention of catastrophic failure. For this purpose, a single fiber reflectance spectrometer was embedded in cement paste samples for the monitoring of water at the fiber tip through its sensitivity to changes in the refractive index. It monitored the curing of samples with different water-to-cement ratios (w/c), between 0.45 and 0.60, measuring the water exhaust during the hardening of the cement paste. It also measured the capillary coefficient from cement paste samples of 0.50, 0.55 and 0.60 w/c : 0.668 ± 0.002 mm/ \sqrt{h} , 1.771 ± 0.052 mm/ \sqrt{h} and 6.360 ± 0.269 mm/ \sqrt{h} , respectively. The capillary coefficient values agree with gravimetric measurements of sorptivity and are further confirmed through porosity measurements made with a scanning electron microscope. Thus, single fiber reflectance spectroscopy can be a gateway to inexpensively measure the entire life cycle of cement, from its curing until its eventual decay, assessing, in situ, its durability through the capillary coefficient.

Keywords: fiber optic sensor; cement paste; cure; hydration; durability; permeability; real-time monitoring; capillary coefficient



Citation: da Silva, P.M.; Coelho, L.C.C.; Almeida, J.M.M.M.d. Single Fiber Reflectance Spectroscopy for the Monitoring of Cement Paste. *Chemosensors* **2021**, *9*, 312. <https://doi.org/10.3390/chemosensors9110312>

Received: 14 September 2021
Accepted: 1 November 2021
Published: 4 November 2021

Publisher's Note: MDPI stays neutral with regard to jurisdictional claims in published maps and institutional affiliations.



Copyright: © 2021 by the authors. Licensee MDPI, Basel, Switzerland. This article is an open access article distributed under the terms and conditions of the Creative Commons Attribution (CC BY) license (<https://creativecommons.org/licenses/by/4.0/>).

1. Introduction

Reinforced concrete has been a go-to for infrastructure and housing projects in the last century and is paramount for our developed society. Most of our infrastructure has been built in the past 50 years with a service life of 50–100 years [1], creating a demand for their monitoring. Concrete on its own is capable of withstanding large compressing forces. However, it requires embedded steel beams to minimize cracking under tensile forces [2].

The properties of concrete are established early on during the hydration of cement and depend on the water-to-cement ratio (w/c), the type of cement used, the added aggregates or pozzolans and the curing methods employed [3,4]. Cement curing has five different stages: Mixing, dormancy, hardening, cooling and densification [3]. In mixing, the dissolution of cement grains occurs in a brief exothermic reaction, during which the formation of ettringite restricts the further dissolution of cement grains. Thus, cement advances to the next phase of hydration—dormancy. This lasts between two to four hours, whilst water begins to be saturated with calcium and hydroxide ions. Eventually, this triggers the formation of calcium–silicate–hydrate (C-S-H) and calcium hydroxide (CH) in an exothermic reaction, causing the cement to become stiffer—hardening. These hydration products, C-S-H and CH, begin to limit the dissolution of cement, which lowers its temperature—cooling. Over time undissolved cement continues to hydrate, leading to its densification.

Porosity is heavily dependent on the w/c . The same volume of cement powder generates a larger volume of cement paste the more water is used during mixing. However, it also results in a more porous material [5]. Hence, a higher w/c equates to a more porous paste, better capillary continuity and better overall cement permeability. For 0.40, 0.50, 0.60 and 0.70 w/c the expected porosity is 11%, 22%, 30% and 37%, respectively [5]. The interlink between pores is not static, e.g., while the capillaries from a 0.45 w/c paste are expected to become discontinuous after seven days, it will take six months for the same to happen for a 0.60 w/c paste [3].

Over time, cement's porosity as well as the formation of small (30–50 μm) to large (>150 μm) cracks lead the way for the decaying of reinforced concrete structures (RCS) [6]. Carbonation [7] and chloride ion ingress [8] destroy the passivation of the embedded steel beams while freeze-thaw [9] and alkali-silica reaction [10] negatively affect the cement paste.

Monitoring RCS is fundamental to prevent catastrophic failures and optimize their expensive repair. Optical fiber sensors were applied for this purpose because they are light, small, resistant and impervious to electromagnetic interference. They were used to measure temperature, strain and relative humidity using fiber Bragg gratings and/or long period fiber gratings [11–14]. pH measurements, indicative of carbonation, also proved fruitful [15], making use of multimode fibers with pH sensitive polymers in their tip. Non-reversible optical fiber sensors were, also, produced for the monitoring of chloride ion ingress [16,17].

The availability of water is a key factor in the life cycle of cement, being the driving force of curing [3], self-healing [18] and a requirement concerning many of its decay mechanisms [19]. In the present work, a single fiber reflectance spectrometer [20] is proposed for the monitoring of water in cement curing and, once hardened, in the pores. Thus, we present a solution that allows the monitoring of cement's full life cycle, which could prove valuable for the monitoring of RCS given that cement is one of its major constituents. We found single fiber reflectance spectroscopy to be successful in achieving the capillary coefficient of cement paste, a parameter through which the durability of cement can be estimated. These values were compared to the sorptivity and the porosity of the samples achieved through gravimetric measurements of water uptake and using scanning electron microscope, respectively, as seen in the following sections.

1.1. Single Fiber Reflectance Spectroscopy

In single fiber reflectance spectroscopy, light from a broad-band light source travels through the first branch of a bundle of two multimode fibers into a larger, sensing, multimode fiber. At the distal end of the sensing fiber, light is reflected back into the bundle, being measured by a spectrometer at the end of the second multimode fiber, Figure 1a.

The reflection of light on the fiber tip is dependent on the refractive index (RI) of the fiber core ($n_c = 1.4584$ at 589.29 nm) and the RI of the external medium (n_p), Equation (1). For cement, n_p depends on how the pores are filled; if they are filled with water n_p is 1.3325; if they have no water at all, n_p will be 1.0. Generally, the RI will be in between these two values with some pores being filled, some being partially filled and the others empty [21]. Due to the durability of cement, we consider that throughout a single measurement of water uptake, there will not be enough change concerning the cement to introduce noise into the monitoring of the capillary coefficient, whether that be through changes in the refractive index of its constituents or micro/macro-mechanical changes in the cement matrix.

$$R_{\text{pore}} = \frac{(n_c - n_p)^2}{(n_c + n_p)^2} \quad (1)$$

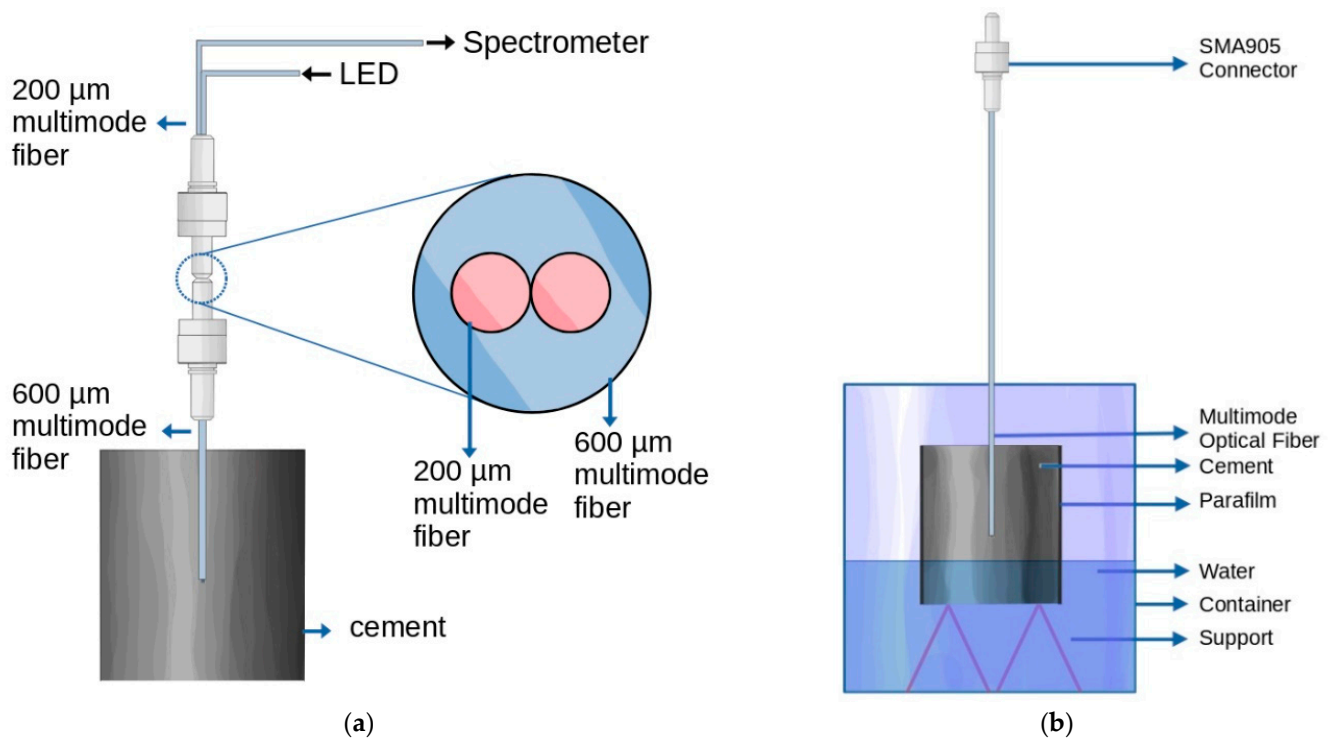


Figure 1. (a) Scheme of single fiber reflectance spectrometer embedded in cement paste. Light is emitted from an LED to a 200 μm multimode fiber, travels to a sensing 600 μm multimode fiber, where it is reflected at the fiber tip into a 200 μm multimode fiber and acquired by a spectrometer. (b) Sorptivity test with part of concrete sample submerged underwater with its sides covered with parafilm. The bottom face of the sample is in contact with water and the top is exposed to air. The SMA905 connector is shown, but it is not used; only the weight of the sample is measured.

This type of sensor is typically used to study changes in the spectrum of reflected light after its interaction with a sample, e.g., human skin [22]. Here it is employed for the monitoring of water during cement curing, and, once hardened, in the cement paste. The porosity of cement paste influences the sensor's sensitivity, with changes in porosity and pore connectivity equating changes in the sensor's response.

1.2. Capillary Coefficient and Sorptivity

The capillary coefficient is a parameter that defines the rate of water uptake of a porous material and has been used as a measure of concrete durability [23,24]. To achieve this value a water absorption test is conducted where the bottom face of a concrete sample is under water and the upper face is in open air. The sides of the sample should be impermeable, thus allowing water to travel in a single direction, vertically. The driving force of capillary absorption is surface tension on fine pores (10 nm–10 μm), which matches the gravity forces of water. The one-dimensional movement of water is described by the Lucas–Washburn equation [25]:

$$h = k\sqrt{t} \quad (2)$$

where h is the height reached by water, k is the capillary coefficient and t is the time. If one measures the volume of water that is being absorbed by the sample per unit of cross section, the water absorption is described by a similar formula, Equation (3) [25]:

$$I = S\sqrt{t} \quad (3)$$

where I is the volume of absorbed water per unit of cross section, S is the sorptivity and t is the time. Figure 1b displays how the samples containing a sensing multimode fiber were set for the measuring of sorptivity. Measuring k requires robust technologies, such as: Neutron radiography, nuclear magnetic resonance, gamma ray or X-ray computed tomography. This

makes measuring S more attractive, since it is achieved through gravimetric measurements, even though the relationship between k and concrete's durability is easier to attain [26]. Both k and S have the same dimensions [$LT^{-\frac{1}{2}}$], but they are not the same thing, with sorptivity containing information of concrete's porosity (φ), Equation (4) [26]. This equation opens the possibility to cross-reference capillary coefficient values with sorptivity values provided the w/c ratio or the porosity of cement are known. These measurements can also be employed to cement pastes, as seen below.

$$\frac{S}{k} = \varphi \quad (4)$$

In these tests it should be assumed that concrete is fully matured, meaning that only a small amount of water will be lost to chemical interactions with the cement paste [23]. If this is not the case, other solutions that do not interact with cement could be used: Water saturated with $\text{Ca}(\text{OH})_2$ [24].

1.3. Scanning Electron Microscope

In the Scanning Electron Microscope (SEM) a beam of electrons undergoes a series of inelastic and elastic collisions which generate a signal that is detected and transformed into an image [27]. In inelastic collisions, incident electrons knock out electrons of atoms in the sample, with the latter having lower energy. The signal from these low energy electrons constitutes the secondary electrons (SE) where only those from the near surface can escape, making it a high-resolution method for the measurement of the topography of the sample. In SE, the edges from a rough surface are brighter since they have more area from which electrons can escape.

Electrons that experience elastic collisions, backscattered electrons (BSE), retain their energy, thus they can escape from greater depths of the sample. The brightness from these images is related to the atomic number of the atoms in the sample. A higher atomic number leads to more collisions, hence a brighter spot. In a polished piece of cement, anhydrous cement appears brightest, followed by calcium hydroxide, calcium silicate hydrate and ettringite. Porosity lowers the atomic size within a phase, making it darker, with voids being black [28].

2. Materials and Methods

2.1. Experiment Setup

A multimode fiber was illuminated with a UV LED (ultra-violet light emitting diode) of 370 nm (XSL-370-TB-5, Roithner LaserTechnik GmbH, Vienna, Austria) and the reflected spectra was acquired with a micro spectrometer (C12880MA MEMS, Hamamatsu, Shizuoka, Japan). A pair of 200 μm multimode fibers connected the LED and the spectrometer to a 600 μm multimode fiber that was embedded in the cement paste, Figure 1a.

An ATmega328P was used to control the LED and the spectrometer, Figure 2a and the data were sent to a computer via USB (Universal Serial Bus) using UART (Universal Asynchronous Receiver-Transmitter). The spectrometer is connected to the microcontroller unit (MCU) through a breakout board [29]. The acquisition procedure makes use of the code provided by the breakout board manufacturer [30] to retrieve the spectrum from the spectrometer: `readSpectrometer()` sends the data from the spectrometer to the MCU and `printData()` sends it from the MCU to a computer via UART.

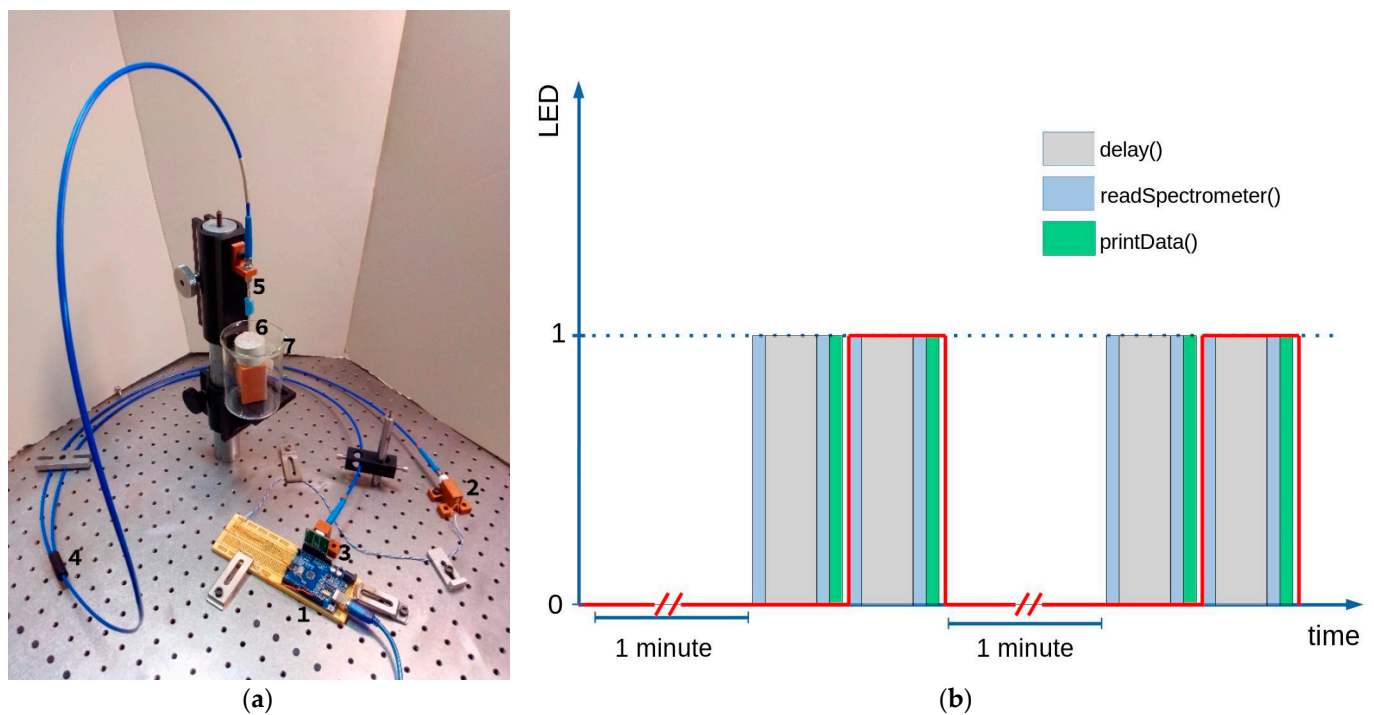


Figure 2. (a) Experimental setup for the monitoring of the cure and capillary coefficient of cement used during this work with a (1) microcontroller, (2) LED, (3) spectrometer, (4) 200 μm multimode fiber bundle, (5) sensing 600 μm multimode optical fiber, (6) cement paste sample and (7) recipient with water. (b) Graphical display of the MCU code, with one-minute pauses between readings, the sensor is reset by reading its stored values, followed by the integration time, e.g., a 200-millisecond delay, for the dark spectrum and the reflected light spectrum, which are measured and sent to a computer via UART.

2.2. Acquisition Scheme

This spectrometer does not have a shutter, but even if the entire system were completely isolated, there would be an ever increasing dark current in between readings. Consequently, a simple way of using this sensor is to continuously acquire and send data with only a small, but consistent, pause between spectrum readings. This would mean that both the spectrometer and the ATmega328P will be continuously working even if the data ends up not being used. Moreover, the data management will fall on the computer on the other side of the UART communication. Since the aim of the sensor is the in situ measurement of the capillary coefficient of RCS, energy needs of the system must be taken into account. Thus, the sensor should acquire data sporadically and not continuously, which in this case means data are retrieved every minute. During the one minute pause the sensor will fill up in charge. For this reason, we cleared the spectrometer by making a reading before the integration time (e.g., 200 milliseconds for sample B) of the measurement. At the end of each one-minute interval two spectrums were measured—a dark one and one with the reflected light from the LED, Figure 2b.

2.3. Sample Preparation

The distal ends of SMA905 connectorized multimode fibers of 600 μm were embedded during the curing of several samples of cement paste with w/c between 0.45 and 0.60 w/c , Table 1. The capillary coefficient was achieved by submerging the samples (wet/dry cycles) and monitoring the water filling up the capillary pores through changes in reflectance at the optical fiber tip, Figure 3a. In these samples the parafilm was placed in the bottom face of the cement paste to allow the water intrusion to be parallel to the optical fiber tip surface. Water moves from the sides of the sample inward.

Table 1. Cement paste samples used for the cure and wet/dry cycle monitoring.

Sample Name	w/c	Cure Time (days)	Cure Monitoring	Wet/dry Monitoring	Shape	Size $\varnothing \times h$ (cm)
A	0.45	3	Yes	No	sphere	2.49 \times -
B	0.50	7	Yes	Yes	cylinder	3.46 \times 1.77
C	0.55	3	No	Yes	cylinder	3.48 \times 2.59
D		1	Yes	No	cylinder	3.45 \times 2.87
E	0.60	3	Yes	No	sphere	2.46 \times -
F		3	No	Yes	cylinder	3.48 \times 2.52

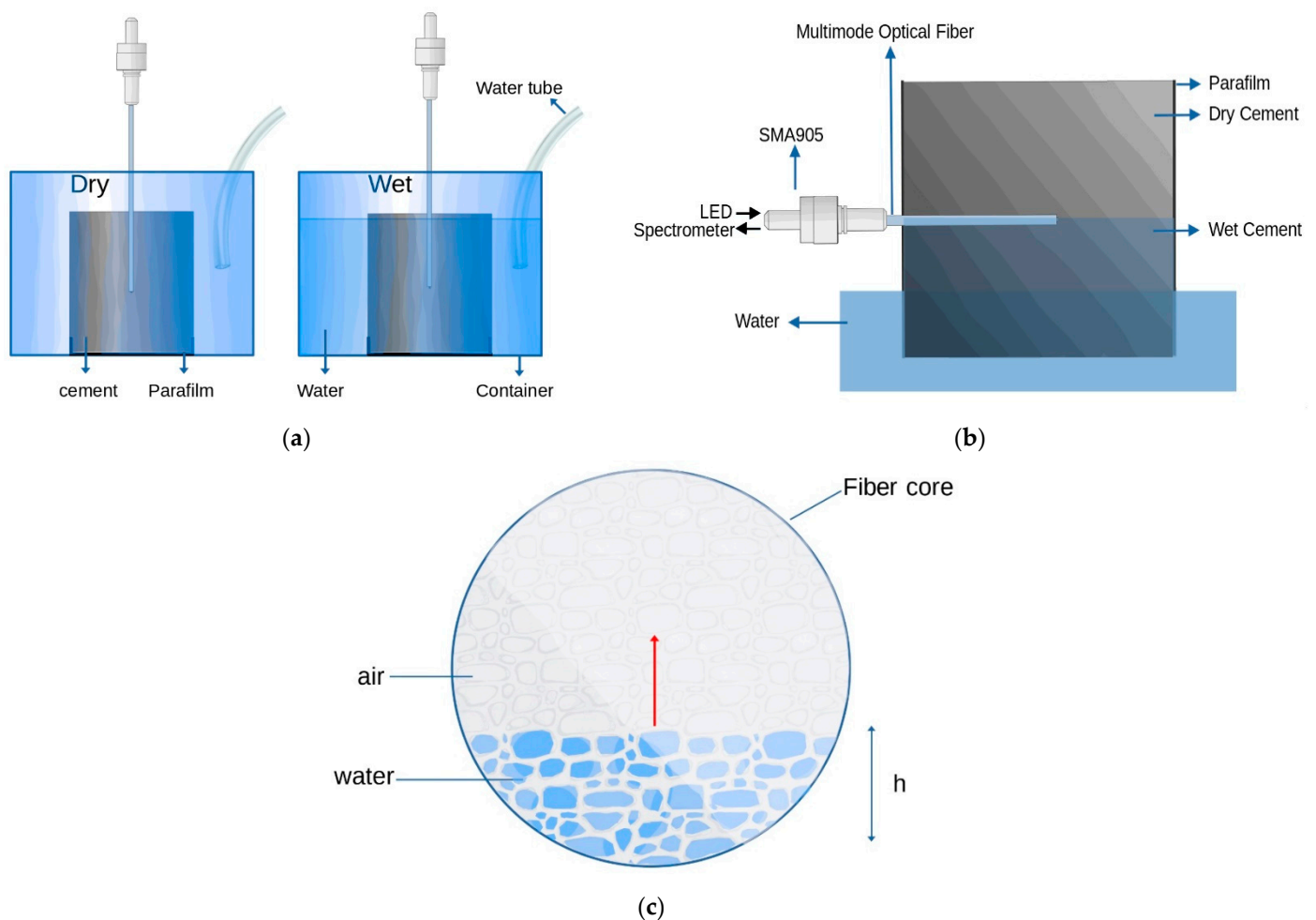


Figure 3. (a) Wet/dry cycle scheme where a plastic tube is used to add and remove water from the recipient and the bottom of the sample is sealed with parafilm. (b) Fiber core embedded in concrete with a point of view of the fiber tip illustrated in (c), with height, h , reached by water in the pores. The red arrow is the direction of water ingress.

Most of the samples were cured for three days in a mold sealed from the outside environment with water being added after the first twenty-four hours. The only exceptions were the 0.50 w/c sample B, which was cured for seven days with water being added two times during this period. And sample D (0.55 w/c), which was cured unsealed from the outside environment, allowing photos of the cement paste to be taken. As well as, the extraction of 0.5 grams of cement paste for the topography analysis of cement particles through SEM. This was done with the objective of seeing the exhaust of φ and the

formation of C-S-H and CH during the hydration of cement. Half grams of cement were extracted from sample D 1 h and 45 minutes, 3 h and 4 minutes and 5 h and 58 minutes after the start of the sample's hydration. The extracted cement was submerged in ethanol for one day with ethanol being renewed after 1 h. After the first 24 h, the ethanol was removed, and the samples were stored in a container with silica-gel to prevent contamination from ambient humidity. A small part of these samples was then placed in carbon tape with its cement particles being observed through SEM (FlexSEM 1000, Hitachi High-Tech, Tokyo, Japan) in SE mode. The samples whose capillary coefficient was measured were broken up to estimate their porosity through SEM by means of BSE.

2.4. Capillary Coefficient and Calibration

Looking through the cement into the fiber tip embedded in it, with water moving in a single direction as in Figure 3b, it would be possible to see water filling through the pores from the bottom of the circle upwards to its top, as seen in Figure 3c. The area of the fiber in contact with air will be proportional to our signal, the latter being the sum of the spectrum of the reflected light. The area of the fiber tip in contact with water is related to the height of the water at the fiber tip, through Equation (5).

$$\alpha = \cos^{-1}\left(\frac{0.3 - h}{0.3}\right) \quad (5)$$

$$A = \frac{0.283\alpha}{\pi} - (0.3 - h) * 0.3 * \sin(\alpha)$$

Here, α is the angle the center of the fiber tip makes with the intersections of the water level and its circumference. h is the height of the water, 0.3 is the radius of the fiber in mm, 0.283 is its area in mm² and A is the area covered with water. The intensities measured in the wet/dry cycles were normalized to the area of the fiber tip and converted to the height of water through a conversion table, populated using Equation (5). Assuming that the movement of water around the optical fiber tip is one dimensional and parallel to the fiber tip surface, a good estimate of the capillary coefficient can be achieved from the slopes of the height of the water as a function of the square root of time in the "wet" cycles.

It is important that the time is reset in the estimation of each of the slopes, with the start being the beginning of the signal drop, indicating that water has reached the fiber tip. This deviates from the measurement of the capillary coefficient, which begins the moment water is in contact with the sample. With the fiber tip we can only see part of this measurement, as seen in Figure 4a,b. A fiber that is next to the surface of the sample that is in contact with water can make the proper estimation of the capillary coefficient, through Equation (2), since the signal drop coincides with the submersion of the sample. Applying Equation (2) to the signal from fibers 2 and 3 of Figure 4b will lead to an underestimation of the capillary coefficient.

The relationship between the distance of the fiber tip, and its error in the estimation of the capillary coefficient can be seen on the curves of Figure 4c. In this case the distance from the fiber tip to the surface of the sample that is in contact with water is known. We can use these distances to plot calibration curves that yield the true value of the capillary coefficient from the measured ones, Figure 4d. These curves are plotted using the values at 0 mm in the graph of Figure 4c and plotting them as a function of the values at 12.0 (sample B), 13.8 (sample C) and 16.2 (sample F) mm of the same graph. Thus, the calibration curves for samples B, C and F are, respectively, $5.346x - 2.85 \times 10^{-3}$, $5.723x - 2.67 \times 10^{-3}$ and $6.189x - 2.17 \times 10^{-3}$.

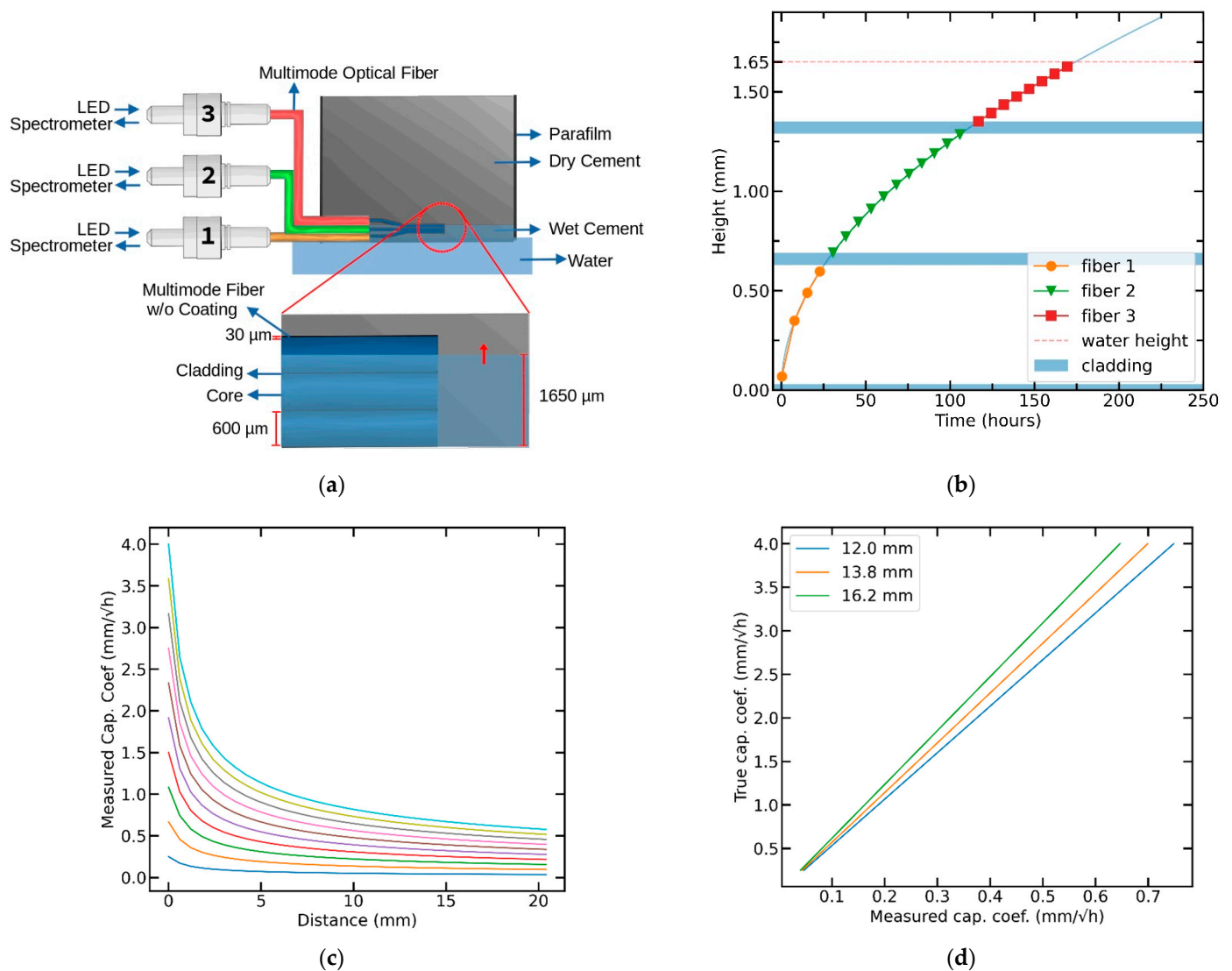


Figure 4. (a) Optical fibers at different distances from the surface and (b) their respective measurements of water height as a function of time. (c) Influence of the distance between the fiber tip and the surface of the sample in contact with water on the measured capillary coefficient. (d) Calibration curves for the optical fiber tips used in 0.50 (sample B), 0.55 (sample C) and 0.60 (sample F) w/c cement paste, which are, respectively, 12.0, 13.8 and 16.2 mm from the surface.

2.5. Validation and Noise Estimation

To verify the estimated capillary coefficient, gravimetric measurements of the sample's sorptivity were made according to Figure 1b. Parafilm was used to seal the sides of the sample and the recipient was filled with water until about 5 mm of the sample was covered with water. In each measurement of the sample's weight, the excess water from the bottom and side surfaces of the cement paste was removed beforehand. Through Equation (4), the porosity of the samples can be assessed and ultimately confirmed using SEM. Five BSE images were taken for each sample of cement paste, achieving a viewing area of 0.024 mm^2 . Each pixel had 8 bits of brightness information, 0 being dark and 255 being white. The images were cleaned using a gaussian filter to remove some of the graininess and a threshold of $30/255$ was chosen, below which the pixels are dark enough to be considered pores. The contrast and brightness setting of the SEM were kept the same with only the focus being adjusted between measurements.

The signal-to-noise ratio of the system was calculated by removing the shape of the data through a Savitzky–Golay filter (see Figure 5) calculating the standard deviation of

the noise (σ) and using it to divide the mean value of the signal (μ), Equation (6). Figure 5 has the signal drop from a 0.6 w/c sample (F) submerged in water, complemented by two spectra, one from a data point before the water has reached the fiber tip—higher light intensity; and another for cement that is saturated with water—lower light intensity. Each data point was achieved by summing the individual intensities from the wavelength between 350 and 390 nm.

$$\text{SNR} = \frac{\mu}{\sigma} \quad (6)$$

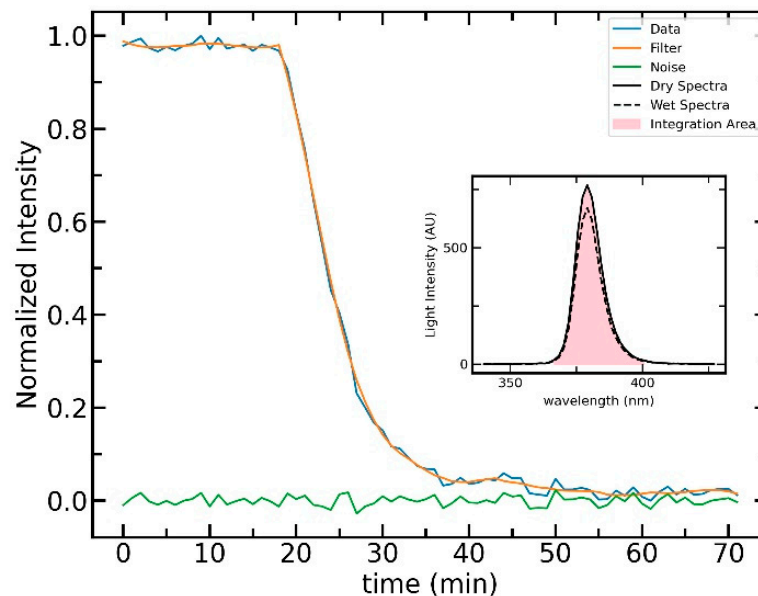


Figure 5. Scheme of the signal-to-noise computation of the signal (blue) with a Savitzky–Golay low-pass filter (orange) to separate the shape of the signal from its noise (green). The inset represents the wavelength from the UV-LED (370 nm) in black, with the integration area (pink) over which the data points are obtained.

3. Results

A single fiber reflectance spectrometer was used to monitor both the cure and wet/dry cycles of a cement paste sample of 0.5 w/c , sample B. The data acquisition lasted for fifteen days of continuous monitoring (see Figure 6a) with another wet cycle being done a week later (see Figure 6b), resulting in a total of eighteen days of observation. The curing of samples A, D and E with, respectively, 0.45, 0.55 and 0.60 w/c were monitored. Samples C and F with w/c of 0.55 and 0.60 were submerged in water once to estimate the capillary coefficient from the water ingress.

From all the data acquired, the worst signal-to-noise ratio was 18, measured in the “wet” cycle of the samples C and F with 0.55 and 0.60 w/c , Table 2. The low SNR of samples C and F can be explained by the non-optimization of the integration time for these measurements. The small integration time employed led to a small amount of signal reaching the spectrometer, riddling the data with noise.

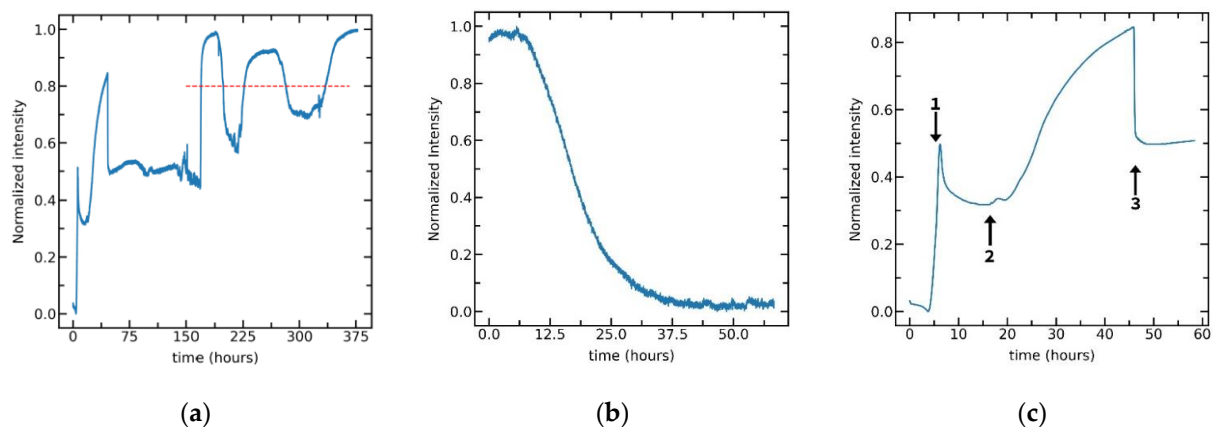


Figure 6. (a) Normalized reflected light intensity over the cure and the “wet/dry” cycles on the cement paste, sample B. (b) Wet cycle made one week later, on the same sample. (c) Normalized reflected light intensity during the first 60 h of the seven-day cure of sample B: (1) Hardening of cement, (2) possible water bleeding and (3) externally added water.

Table 2. Signal-to-noise ratio (SNR) for each of the tests undertaken during this study.

Sample Name	w/c	Test	SNR
A	0.45	Cure	220
		Cure	87
B	0.50	Wet/Dry	60
		Wet	608
C	0.55	Wet	18
D	0.55	Cure	253
E	0.60	Cure	34
F		Wet	18

3.1. Cure

According to Figure 6c, concerning the curing of sample B, in the first 3 h there was a slight decrease in reflected light followed by a step increase from 3 to 6 h, point 1 of the figure. The step increase is also found in samples A, D and E in Figure 7a and happens at the same time as the samples become visibly stiffer (Figure 7d), indicating that the cement is transitioning from dormancy to its hardening phase. This is corroborated by SEM images acquired through SE from cement extracted during the curing of sample D, Figure 7b–d. The SEM images of Figure 7b,c have particles of cement with little to no formations of C-S-H at the surface, in stark contrast with Figure 7d where the particle’s surface is more uneven. This time frame agrees with the two to four hours the dormancy phase is expected to last [3].

The depletion of water in the fiber vicinity is temporarily reversed between 6 and 16 h in sample B, Figure 6c. This could be due to water bleeding, a common feature during cement hydration, where large aggregates could accumulate water underneath them [5]. This did not happen for samples A and E, whose intensity kept increasing, indicating further depletion of water. The excess water ended up being used by 41 h and water was added externally to aid the curing of cement with it remaining saturated for the remainder of the curing. In this saturated state, the normalized intensity is between 44 and 59%. At the end of the seven days (168 h), sample B was removed from the mold and left to dry, leading to a fast increase in reflected light intensity, Figure 6a.

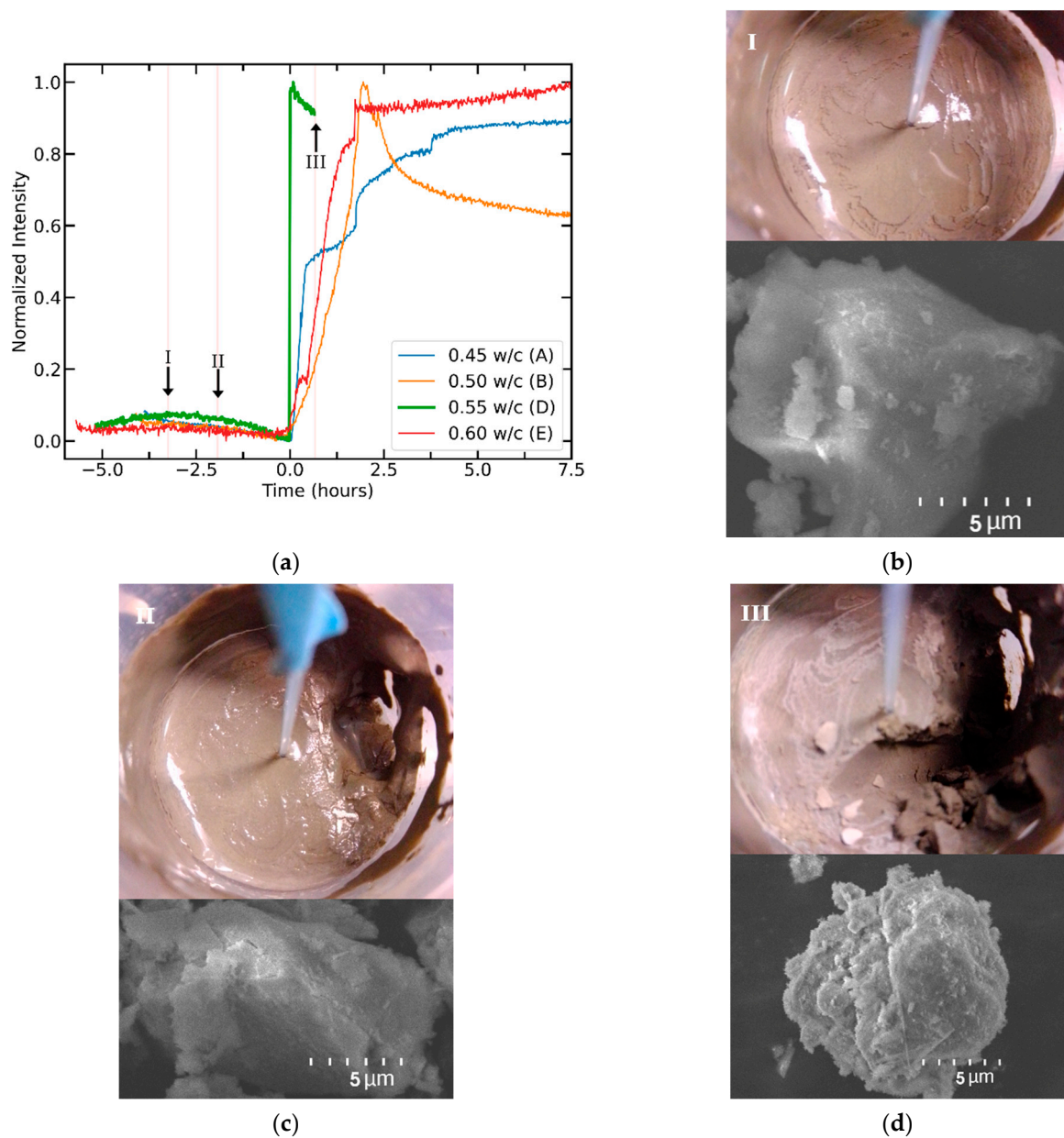


Figure 7. (a) Reflected light intensity from the curing of samples A, B, D and E with w/c of 0.45, 0.50, 0.55 and 0.60, respectively, accompanied by images from the cure and particles (SE images) of sample D at 1 h and 45 minutes (b), 3 h and 4 minutes (c) and 5 h and 50 minutes (d) after the beginning of the curing.

3.2. Wet/Dry Cycles

Once sample B was dry, it underwent wet/dry cycles to access the sensor's response. It is clear in Figure 6a,b that the wet cycles led to a reduction in the reflected light on the fiber tip, while the dry cycles led to an increase. The signal for saturated cement paste went from 44% at the end of the curing, to 56% in the first wet cycle and 68% in the second. For the dry cycle, the planes were at 98%, 92% and 100%. Two separate zones of reflected light intensity, one for mostly dry cement paste and another for wet cement paste were found, divided by the dashed redline of Figure 6a.

Plotting the wet cycles as the height of water on the fiber tip, deduced from Equation (5), over the square root of time (Figure 8a) and applying the corrections of Figure 4d to the slope values, the capillary coefficient of the sample B was estimated, Figure 8b. There is a decrease of the capillary coefficient between the first and the other two measurements,

decreasing from $1.373 \pm 0.01 \text{ mm}/\sqrt{\text{h}}$ to $0.668 \pm 0.002 \text{ mm}/\sqrt{\text{h}}$ (average of the last two measurements).

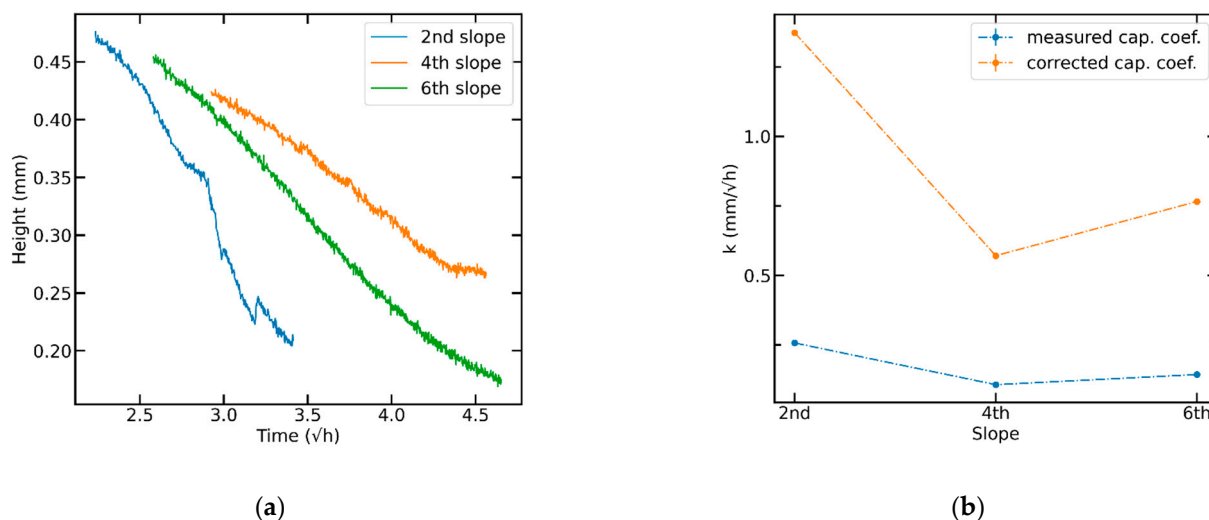


Figure 8. (a) Comparison of the different slopes of the “wet” cycles of sample B plotted as the height of water over the square root of time. (b) The respective capillary coefficients obtained from the “wet” cycle’s slopes and the respective corrected values.

The same procedure was done for the samples of cement paste C and F (Figure 9a,b); as expected, an increase in capillary coefficient with an increase in w/c was found, with values ranging from $1.771 \pm 0.05 \text{ mm}/\sqrt{\text{h}}$ to $6.360 \pm 0.27 \text{ mm}/\sqrt{\text{h}}$ for 0.55 and 0.60 w/c respectively, Figure 9c.

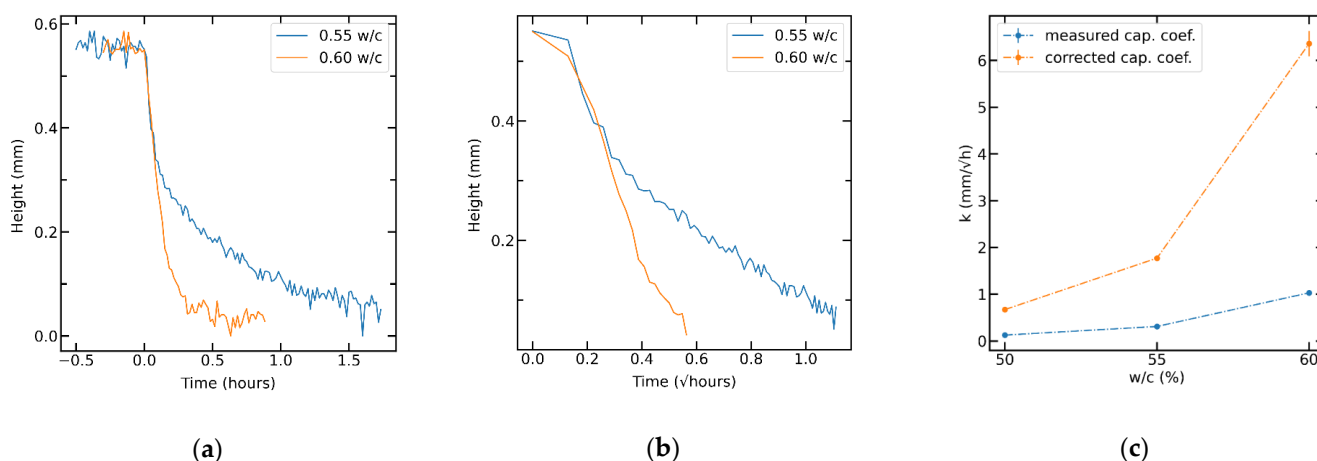


Figure 9. (a) Reflected light intensity for cement paste samples C (0.55 w/c) and F (0.60 w/c) converted to height of water at the fiber tip through Equation (5). (b) Slopes of the height as a function of the square root of time and (c) measured capillary coefficient for samples B (0.50 w/c), C and F, and their corrected values using the slopes of Figure 4d.

3.3. Samples’ Sorptivity and Porosity

Gravimetric water absorption tests (Figure 1b) were conducted to estimate the sorptivity value of samples B, C and F, with the obtained data in Figure 10a. An increase in sorptivity was found the higher the w/c with samples B (0.5 w/c), C (0.55 w/c) and F (0.60 w/c) having, respectively, sorptivity values of $0.131 \pm 0.004 \text{ mm}/\sqrt{\text{h}}$, $0.505 \pm 0.080 \text{ mm}/\sqrt{\text{h}}$ and $2.290 \pm 0.110 \text{ mm}/\sqrt{\text{h}}$.

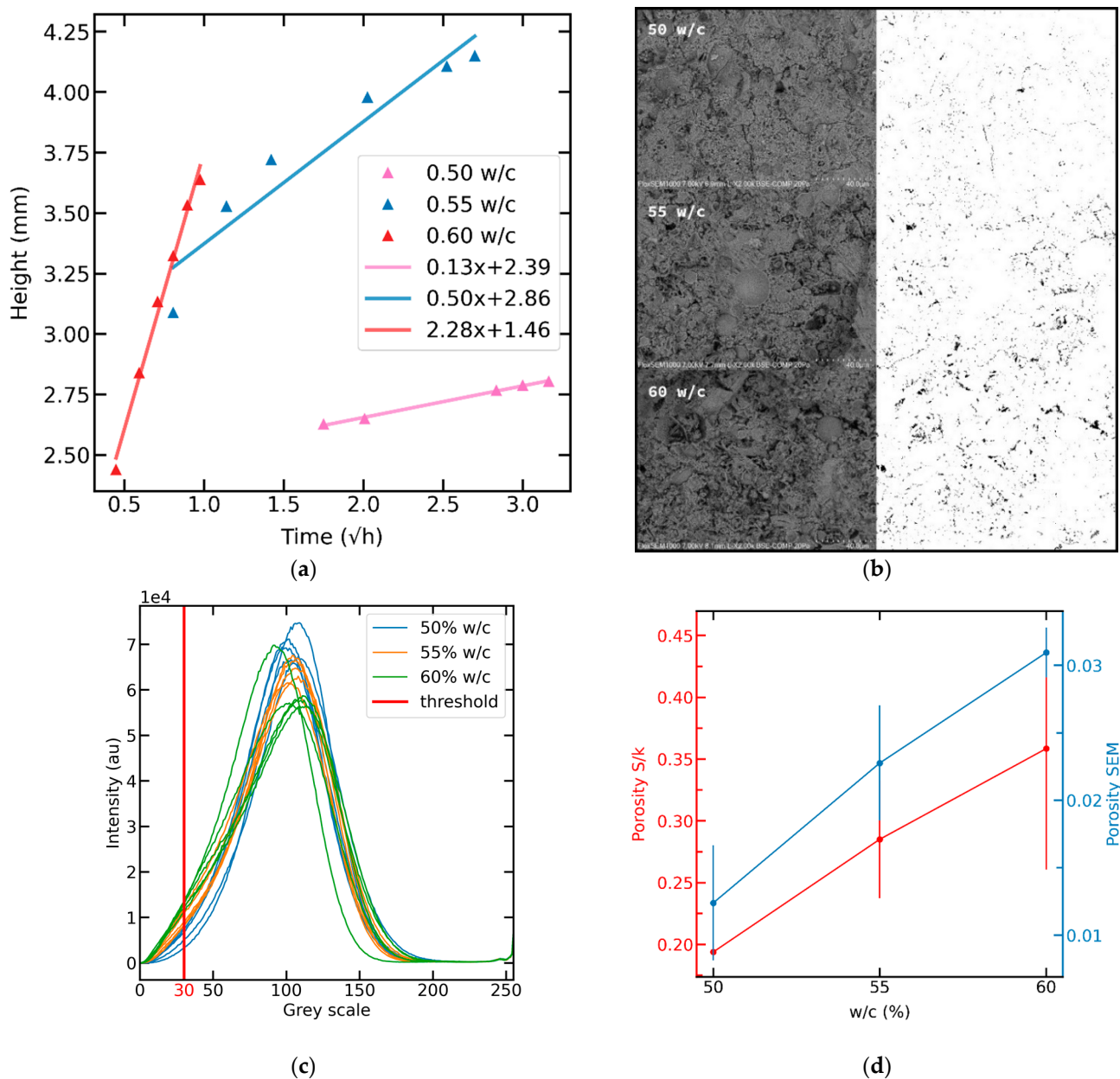


Figure 10. Volume of absorbed water per unit cross section over the square root of time for samples B (0.50 w/c), C (0.55 w/c) and F (0.60 w/c) (a). SEM BSE images filtered with a Gaussian filter for samples B, C and F on the left and their porosity on the right (b). (c) Histograms of the grey scale of the images acquired through SEM and the 30/255 threshold in red. (d) Comparison of the porosity achieved through SEM and through Equation (4).

Using the corrected values of the capillary coefficient and these values of sorptivity, Equation (4) is used to achieve the porosity of the samples used: $19.4 \pm 0.6\%$ (sample B), $28.5 \pm 4.8\%$ (sample C) and $35.9 \pm 9.8\%$ (sample F). These porosity values are close to the expected ones [5], meaning that both the capillary coefficients from the single fiber reflectance spectrometer and the sorptivity values are in agreement.

BSE images from SEM were used to confirm the porosity achieved previously. These images will not yield the true porosity of the samples, but they can be used to compare the porosity between samples [27]. Figure 10b has BSE images that went through a Gaussian filter on the left and their porosity, pixels with brightness below 30 in 255, on the right. It is possible to see from this image alone that there is an increase in porosity with an increasing w/c. The histograms of the scale of grays for the images taken, five for each sample, can

be seen in Figure 10c along with the chosen threshold (30/255). Figure 10d compares the porosity achieved through the relationship of Equation (4) and the one measured through SEM. Both curves are extremely similar, having between them a Pearson product–moment correlation coefficient (ρ) of 0.99998.

4. Discussion

Monitoring the availability and the mobility of water in concrete is key in estimating the decaying rate of cement paste; thus, this has been one of the objectives of many previous studies [19]. In this work the use of single fiber reflectance spectroscopy achieved valuable information for both the curing of the cement as well as for hardened cement paste. It is important to note that in single fiber reflectance spectroscopy water ought to be transparent to the chosen wavelength of the light source. Thus, theoretically, the measured light intensity should be only sensitive to changes in the refractive index at the fiber tip. This way, light that goes out of the fiber and bounces back into it from the cement paste is the same regardless of the portion of fiber tip in contact with water. Water is highly transparent to visible light, which broadens the pool of available light sources. A wavelength of 370 nm was chosen due to convenience and, despite the absorption at this wavelength being higher— $1.37 \times 10^{-3} \text{ cm}^{-1}$ —than the optimum value of $2.5 \times 10^{-4} \text{ cm}^{-1}$, at 475 nm [31], the loss of signal at the vicinity of the fiber tip due to water absorption remained negligible: Considering an extreme case where there is gap of 0.5 cm between the fiber tip and the cement paste, the loss of signal due to water absorption would require an SNR of 730 to be measured. Even in this case, that value is greater than any other SNR achieved in this study, Table 2.

This sensor was sensitive to the hardening of different samples of cement paste (Figure 7a–d), a key mark of the cement’s hydration. At point 3 of Figure 6c, an excessive amount of water was added, which left the sample saturated. Since the addition of water during the cement’s curing is one of the methods used to improve cement paste’s cohesion [3], the monitoring of this procedure is an important feature of this sensor. This could enable the user to fine tune the amount of water and the timing of its addition.

The sensor can monitor the absorption of water in cement paste as seen in Figure 6a,b, but its information on the amount of water in cement paste shows strong variability for sample B: Saturated cement paste had its signal change from 44% to 68%, while dry cement paste was between 92% and 100%. This is to be expected since over the lifetime of cement paste there are changes in the pore size and connectivity that may lead to the trapping of water and/or air in the cement paste that is in the vicinity of the fiber tip. This is especially important to consider during these measurements since we used recently made cement paste. There is, still, cement to be hydrated and for 0.50 *w/c* cement paste the breakage of pore connectivity is expected within the first 28 days [3]. This variability is, also, to be expected in fully matured paste, since the cement paste that surrounds large aggregates (interfacial transition zones), in this case a multimode optical fiber, is different from the bulk cement paste: It is more brittle and with larger pores [5]. Still, it is reasonable to assume that for values of reflected light above 80%, in Figure 6a, the cement paste is mostly dry and below this value the cement paste is mostly wet.

Transforming the reflected light intensity to height of absorbed water through Equation (5) an estimation of the capillary coefficient was achieved from the slopes of the plot in Figure 8a, as seen in Figure 8b. These values were then corrected using the calibration slope of Figure 4d. The decrease of the capillary coefficient from the first measurement to the last two, from $1.373 \pm 0.010 \text{ mm}/\sqrt{\text{h}}$ to $0.668 \pm 0.002 \text{ mm}/\sqrt{\text{h}}$, strengthens the idea that there is a reduction in the pore size and connectivity. This is likely due to loss of pore connectivity as well as the further hydration of anhydrous cement. Submerging samples C and F yielded a capillary coefficient of $1.771 \pm 0.010 \text{ mm}/\sqrt{\text{h}}$ and $6.360 \pm 0.269 \text{ mm}/\sqrt{\text{h}}$, which are expected values since the capillary coefficient is expected to increase with increasing *w/c*.

The sorptivity values achieved, 0.131 ± 0.004 mm/ \sqrt{h} , 0.505 ± 0.080 mm/ \sqrt{h} and 2.290 ± 0.110 mm/ \sqrt{h} , through gravimetric measurements of samples B, C and F (Figure 10a) corroborate the capillary coefficients reached with the single fiber reflectance spectrometer, resulting, through Equation (4), in porosity values of $19.4 \pm 0.6\%$, $28.5 \pm 4.7\%$ and $35.9 \pm 9.7\%$, which are near the expected values [5], and they also increase with increasing w/c . Moreover, measuring the porosity of these samples through SEM, we found that both curves of porosity are identical with $\rho = 0.99998$. Thus, the capillary coefficient values from single fiber reflectance spectroscopy can be used to extract valuable information concerning the concrete's decay.

For future work, the application of hydrogels for improvements in cement curing due to their water retaining properties can intrinsically be studied from this device. Moreover, the hydrogel's usage to promote self-sealing and self-healing could also be monitored in hardened cement [5,17]. This sensor also has the potential to monitor the alkali–silica reaction through its gel since it has an RI of around 1.5 [28].

5. Conclusions

A single fiber reflectance spectrometer was successfully used to monitor the amount of water available in the vicinity of a fiber tip embedded in cement paste. It could sense the water exhaust at the hardening stage of cement hydration in samples with different w/c , as well as the addition of extra water to aid curing the cement paste. This information is invaluable for the tweaking of cement paste's long-term properties.

It continually monitored a sample of 0.50 w/c for 15 days, from the beginning of curing until the end of the wet/dry cycles. The latter contain information on the amount of water absorbed by the sample, as well as the rate of water uptake—the capillary coefficient. The capillary coefficient is also a measure of cement paste durability and the values obtained by the single fiber reflectance spectrometer agree with gravimetric measurements of sorptivity and SEM measurements of porosity for samples of 0.50, 0.55 and 0.60 w/c .

Author Contributions: Conceptualization, P.M.d.S.; methodology P.M.d.S.; software, P.M.d.S.; formal analysis, P.M.d.S.; investigation, P.M.d.S., L.C.C.C. and J.M.M.M.d.A.; writing—original draft preparation, P.M.d.S.; writing—review and editing, J.M.M.M.d.A. and L.C.C.C.; supervision, L.C.C.C. and J.M.M.M.d.A.; All authors have read and agreed to the published version of the manuscript.

Funding: This work has received funding from the project “SolSensors-Development of Advanced Fiber Optic Sensors for Monitoring the Durability of Concrete Structures”, with reference POCI-01-0145-FEDER-031220, supported by the Program Budget: COMPETE-Operational Program Competitiveness and Internationalization-COMPETE 2020 and the Lisbon Regional Operational Program in its FEDER component and by the budget of FCT Foundation for Science and Technology, I.P. Luís Coelho acknowledges the support from FCT research contract grant CEECIND/00471/2017.

Institutional Review Board Statement: Not applicable.

Informed Consent Statement: Not applicable.

Data Availability Statement: The data used in this project as well as a version of the code are available upon request.

Conflicts of Interest: The authors declare no conflict of interest.

References

1. Pacheco-Torgal, F.; Melchers, R.E.; Shi, X.; De Belie, N.; Van Tittelboom, K.; Sáez, A. (Eds.) Fernando Pacheco-Torgal, Introduction. In *Eco-Efficient Repair and Rehabilitation of Concrete Infrastructures*; Woodhead Publishing: Cambridge, UK, 2018; pp. 1–12.
2. McCarter, W.J.; Vennesland, Ø. Sensor systems for use in reinforced concrete structures. *Constr. Build. Mater.* **2004**, *18*, 351–358. [[CrossRef](#)]
3. Taylor, P.C. Chapters 2 & 3. In *Curing Concrete*; CRC Press: Boca Raton, FL, USA, 2013; pp. 7–10, 37–38.
4. Zhang, S.P.; Zong, L. Evaluation of Relationship between Water Absorption and Durability of Concrete Materials. *Adv. Mater. Sci. Eng.* **2014**, *2014*, 650373. [[CrossRef](#)]
5. Mehta, N.; Monteiro, P. *Concrete*; McGraw-Hill: New York, NY, USA, 2006; pp. 24–26, 44–46, 121–131.

6. Mignon, A.; Snoeck, D.; Schaubroeck, D.; Luickx, N.; Dubruel, P.; Van Vlierberghe, S.; De Belie, N. pH-responsive superabsorbent polymers: A pathway to self-healing of mortar. *React. Funct. Polym.* **2015**, *93*, 68–76. [CrossRef]
7. Chang, C.-F.; Chen, J.-W. The experimental investigation of concrete carbonation depth. *Cem. Concr. Res.* **2006**, *36*, 1760–1767. [CrossRef]
8. Khan, M.U.; Ahmad, S.; Al-Gahtani, H.J. Chloride-Induced Corrosion of Steel in Concrete: An Overview on Chloride Diffusion and Prediction of Corrosion Initiation Time. *Int. J. Corros.* **2017**, *2017*, 5819202. [CrossRef]
9. Cai, H.; Liu, X. Freeze-thaw durability of concrete: Ice formation process in pores. *Cem. Concr. Res.* **1998**, *28*, 1281–1287. [CrossRef]
10. Figueira, R.B.; Sousa, R.; Coelho, L.; Azenha, M.; de Almeida, J.M.; Jorge, P.A.S.; Silva, C.J.R. Alkali-silica reaction in concrete: Mechanisms, mitigation and test methods. *Constr. Build. Mater.* **2019**, *222*, 903–931. [CrossRef]
11. Moyo, P.; Brownjohn, J.M.W.; Suresh, R.; Tjin, S.C. Development of fiber Bragg grating sensors for monitoring civil infrastructure. *Eng. Struct.* **2005**, *27*, 1828–1834. [CrossRef]
12. Yeo, T.L.; Cox, M.A.C.; Boswell, L.F.; Sun, T.; Grattan, K.T.V. Optical fiber sensors for monitoring ingress of moisture in structural concrete. *Rev. Sci. Instrum.* **2006**, *77*, 055108. [CrossRef]
13. Venugopalan, T.; Sun, T.; Grattan, K.T.V. Long period grating-based humidity sensor for potential structural health monitoring. *Sens. Actuators A Phys.* **2008**, *148*, 57–62. [CrossRef]
14. Kaklauskas, G.; Sokolov, A.; Ramanauskas, R.; Jakubovskis, R. Reinforcement Strains in Reinforced Concrete Tensile Members Recorded by Strain Gauges and FBG Sensors: Experimental and Numerical Analysis. *Sensors* **2019**, *19*, 200. [CrossRef]
15. Tariq, A.; Baydoun, J.; Remy, C.; Ghasemi, R.; Lefevre, J.P.; Mongin, C.; Dauzères, A.; Leray, I. Fluorescent molecular probe based optical fiber sensor dedicated to pH measurement of concrete. *Sens. Actuators B Chem.* **2021**, *327*, 128906. [CrossRef]
16. Fuhr, P.L.; Huston, D.R.; McPadden, A.P.; Cauley, R.F. Embedded chloride detectors for roadways and bridges. In Proceedings of the Smart Structures and Materials 1996: Smart Systems for Bridges, Structures, and Highways, San Diego, CA, USA, 28–29 February 1996; Matthews, L.K., Ed.; SPIE: Bellingham, WA, USA, 1996. [CrossRef]
17. Fuhr, P.L.; Huston, D.R. Fiber optic chloride threshold detectors for concrete structures. *J. Struct. Control* **2000**, *7*, 77–102. [CrossRef]
18. Gao, M.; Guo, J.; Cao, H.; Wang, H.; Xiong, X.; Krastev, R.; Nie, K.; Xu, H.; Liu, L. Immobilized bacteria with pH-response hydrogel for self-healing of concrete. *J. Environ. Manag.* **2020**, *261*, 110225. [CrossRef]
19. Baroghel-Bouny, V. Water vapour sorption experiments on hardened cementitious materials. *Cem. Concr. Res.* **2007**, *37*, 414–437. [CrossRef]
20. Zhang, X.U. Single fiber reflectance spectroscopy calibration. *J. Biomed. Opt.* **2017**, *22*, 1. [CrossRef]
21. de Burgh, J.M.; Foster, S.J.; Valipour, H.R. Prediction of water vapour sorption isotherms and microstructure of hardened Portland cement pastes. *Cem. Concr. Res.* **2016**, *81*, 134–150. [CrossRef]
22. Zhang, X.U.; Faber, D.J.; Post, A.L.; van Leeuwen, T.G.; Sterenborg, H.J.C.M. RI measurement using single fiber reflectance spectroscopy. *J. Biophotonics* **2019**, *12*, e201900019. [CrossRef]
23. Lockington, D.A.; Parlange, J.-Y. Anomalous water absorption in porous materials. *J. Phys. D Appl. Phys.* **2003**, *36*, 760–767. [CrossRef]
24. Uzoegbo, H.C. Dry-stack and compressed stabilized earth-block construction. In *Nonconventional and Vernacular Construction Materials*; Elsevier: Amsterdam, The Netherlands, 2020; pp. 305–350.
25. Hanžič, L.; Kosec, L.; Anžel, I. Capillary absorption in concrete and the Lucas–Washburn equation. *Cem. Concr. Compos.* **2010**, *32*, 84–91. [CrossRef]
26. Yang, L.; Gao, D.; Zhang, Y.; Tang, J.; Li, Y. Relationship between sorptivity and capillary coefficient for water absorption of cement-based materials: Theory analysis and experiment. *R. Soc. Open Sci.* **2019**, *6*, 190112. [CrossRef]
27. Scrivener, K.; Snellings, R.; Lothenbach, B. Chapter 8. In *A Practical Guide to Microstructural Analysis of Cementitious Materials*; CRC Press: London, UK, 2017; ISBN 9781138747234.
28. Walker, H.N.; Lane, D.S.; Stutzman, P.E. Chapter 14 & 10. In *Petrographic Methods of Examining Hardened Concrete: A Petrographic Manual*; VTRC: Charlottesville, VA, USA, 2006.
29. Hamamatsu C12880MA MEMS u-Spectrometer and Breakout Board. Available online: <https://www.seeedstudio.com/Hamamatsu-C12880MA-MEMS-u-Spectrometer-and-Breakout-Board-p-2916.html> (accessed on 4 May 2021).
30. Groupgets/c12880ma. Available online: <https://github.com/groupgets/c12880ma> (accessed on 4 May 2021).
31. Hale, G.M.; Querry, M.R. Optical Constants of Water in the 200-Nm to 200-Mm Wavelength Region. *Appl. Opt.* **1973**, *12*, 555. [CrossRef]